Quaternary Science Reviews 159 (2017) 1–14

Contents lists available at ScienceDirect

Quaternary Science Reviews

journal homepage: www.elsevier.com/locate/quascirev

Exploring the oxygen isotope fingerprint of Dansgaard-Oeschger variability and Heinrich events

Witold Bagniewski [a, b], Katrin J. Meissner [a, b, *], Laurie Menviel [a, b, c, **]

[a] Climate Change Research Centre, University of New South Wales, Sydney, NSW, Australia
[b] ARC Centre of Excellence for Climate System Science, Australia
[c] PANGEA Research Centre, University of New South Wales, Sydney, NSW, Australia

ARTICLE INFO

Article history:
Received 5 May 2016
Received in revised form
6 January 2017
Accepted 9 January 2017
Available online 19 January 2017

Keywords:
MIS3
Model-data comparison
Heinrich events
Dansgaard-Oeschger cycles
$\delta^{18}O$
AMOC

ABSTRACT

We present the first transient simulations of Marine Isotope Stage 3 (MIS 3) performed with an oxygen isotope-enabled climate model. Our simulations span several Dansgaard-Oeschger cycles and three Heinrich stadials and are directly compared with oxygen isotope records from 13 sediment and 2 ice cores. Our results are consistent with a 30–50% weakening of the Atlantic Meridional Overturning Circulation during Dansgaard-Oeschger stadials and a complete shutdown during Heinrich stadials. We find that the simulated $\delta^{18}O$ anomalies differ significantly between Heinrich stadials and non-Heinrich stadials. This difference is mainly due to different responses in ocean circulation, and therefore climate, impacting oceanic $\delta^{18}O$, while the volume of ^{18}O-depleted meltwater plays a secondary role.

1. Introduction

Several Dansgaard-Oeschger (D-O) cycles and Heinrich stadials occurred during a period known as Marine Isotope Stage 3 (MIS3, 59.4–27.8 ka BP). The causes and mechanisms underlying this climate variability are still debated. It is commonly suggested that iceberg discharges in the North Atlantic and changes in the Atlantic Meridional Overturning Circulation (AMOC) played a crucial role (Broecker et al., 1985). MacAyeal (1993) proposed that internal ice dynamics can trigger Heinrich events and create massive meltwater fluxes. Modelling studies have shown that such meltwater fluxes can abruptly weaken the AMOC, thus leading to a cooling in the North Atlantic during stadials (Rahmstorf, 1996; Ganopolski and Rahmstorf, 2001; Meissner et al., 2002; Menviel et al., 2014). In addition, records of ice rafted debris (IRD) indicate that all D-O stadials during MIS3 were accompanied by iceberg surges (Dokken and Jansen, 1999; van Kreveld et al., 2000; Elliot et al., 2001), and geochemical proxy records suggest that AMOC was weakened during D-O stadials (Keigwin and Boyle, 1999), thus pointing towards a similar mechanism involved during D-O cycles and Heinrich events. Menviel et al. (2014) showed that most of the reconstructed Heinrich and D-O variability in temperature and precipitation can be reproduced by freshwater-driven changes in the AMOC. However, the debate about whether ice sheet changes were the cause or the consequence of changes in circulation remains unsettled. For example, it has been shown that a collapse of the AMOC can induce subsurface warming and trigger ice sheet instabilities (Marcott et al., 2011; Álvarez-Solas et al., 2013), pointing to internal ocean dynamics as a potential driving force (Peltier and Vettoretti, 2014). Alternative hypotheses involve interactions of wind patterns with continental ice sheets (Wunsch, 2006), changes in sea ice (Li et al., 2010) or sea ice-ice shelf fluctuations (Petersen et al., 2013).

One potential approach to distinguish between the suggested mechanisms is to study changes in seawater $\delta^{18}O$ $\left(\delta^{18}O_w\right)$ in the North Atlantic. Indeed, as high latitude precipitation is depleted in ^{18}O, the glacial Northern hemispheric ice-sheets had a $\delta^{18}O$ signature of −20 to −30‰ (Ferguson and Jasechko, 2015). Therefore, contrarily to changes in sea-ice or winds, the addition of ^{18}O-depleted meltwater has a significant impact on North Atlantic

* Corresponding author. Climate Change Research Centre, University of New South Wales, Sydney, NSW, Australia.
** Corresponding author. Climate Change Research Centre, University of New South Wales, Sydney, NSW, Australia.
E-mail address: k.meissner@unsw.edu.au (K.J. Meissner).

http://dx.doi.org/10.1016/j.quascirev.2017.01.007

surface waters and should thus also be reflected in foraminiferal $\delta^{18}O_c$.

Fully coupled three-dimensional isotope-enabled climate models are a recent addition to the large and diverse family of climate models (Lewis et al., 2010; Brennan et al., 2012, 2013; Roche et al., 2014; Bagniewski et al., 2015) and allow a direct comparison between model simulations and proxy data. For example, Bagniewski et al. (2015) used the isotope-enabled University of Victoria Earth System Climate Model (UVic ESCM) to simulate an idealized Heinrich event and separate the resulting foraminiferal δ^{18} O signal into three main contribution factors influencing local seawater: i) δ^{18} O variations due to changes in circulation and climate, ii) δ^{18} O variations due to meltwater of calving icebergs, and iii) temperature changes.

Until recently, simulations of millennial scale variability have been limited to very idealized settings (e.g. Barron and Pollard, 2002; Knutti et al., 2004; van Meerbeeck et al., 2009). Only two previous studies have provided a transient climate simulation for the entire MIS3 period with a 3-dimensional Earth System Model (Menviel et al., 2014, 2015). Here we present transient simulations of MIS3 with the oxygen isotope-enabled UVic ESCM (Brennan et al., 2012, 2013). It is the first time an oxygen-isotope-enabled model is used in a transient simulation of the last glacial period, thus allowing a more comprehensive comparison with paleoproxy records. Following the method in Menviel et al. (2014), MIS3 climate variability is generated by varying freshwater forcing in the North Atlantic. The results from three such simulations with different meltwater rates and different isotopic signatures of meltwater, are compared with two ice cores and thirteen ocean sediment records.

2. Methods

2.1. Model description

We integrated transient simulations for the period 50–28 ka BP with the UVic ESCM, version 2.9. This earth system model of intermediate complexity, described by Weaver et al. (2001), Meissner et al. (2003), Schmittner et al. (2008), and Eby et al. (2009), consists of fully coupled, ocean, atmosphere, land surface, vegetation, sea ice, and sediment components.

The ocean component of the UVic ESCM is a ocean general circulation model (Modular Ocean Model, Version 2 Pacanowski (1995)), with 19 vertical levels varying from 50 m at the surface to 500 m at 5 km depth. It is coupled to a vertically integrated, two-dimensional atmospheric energy and moisture balance model, forced by solar insolation, and present-day reanalysis winds from the National Centers for Environmental Prediction (NCEP) (Kalnay et al., 1996) with superimposed geostrophic wind anomalies (Weaver et al., 2001). Other model components include a dynamic-thermodynamic sea ice model (Semtner Jr., 1976; Hibler III, 1979; Hunke and Dukowicz, 1997), a sediment model (Archer, 1996; Meissner et al., 2012), a land surface scheme, and a dynamic global vegetation model (MOSES/TRIFFID, Meissner et al., 2003). The version of the UVic ESCM used in this study also includes two stable water isotopes, $H_2^{18}O$ and $H_2^{16}O$, which are integrated into the ocean, atmosphere, land-surface, and sea-ice components of the model (Brennan et al., 2012, 2013; Bagniewski et al., 2015), and are exchanged between these components.

All model components have a spherical grid resolution of 3.6° in longitude and 1.8° in latitude. During simulations, the model conserves water, energy, carbon, and oxygen isotopes to machine precision and without flux adjustments.

2.2. Experimental design

Initial conditions for the experiments were obtained by conducting a 6000 year equilibrium spin-up simulation with the UVic ESCM using an orbital configuration corresponding to 50 ka BP (Berger, 1978), atmospheric pCO_2 of 207.1 ppm (Bereiter et al., 2012), increased elevations based on a reconstruction of Northern Hemisphere ice sheets (Abe-Ouchi et al., 2007) and the corresponding ice albedo. The ocean δ^{18} O is initialized at 0.6‰, 0.5‰ above the pre-industrial seawater initial value of 0.1‰, to allow for seawater enrichment due to larger continental ice sheets.

Transient simulations over the period 50–28 ka BP were forced with transient orbital, ice sheet, and atmospheric CO_2 data. Ice sheet orography and albedo were obtained from an off-line ice-sheet model simulation (Abe-Ouchi et al., 2007); atmospheric CO_2 concentrations were based on Antarctic ice core records (Bereiter et al. (2012) for 50–39.9 ka BP, and Ahn and Brook (2014) for 39.9–28 ka BP). As the model does not include an interactive ice sheet, freshwater withdrawing from the ocean during phases of ice sheet growth and freshwater release into the ocean as a result of ice sheet calving and ablation are not simulated prognostically. To mimic the effect of iceberg surges on ocean circulation and seawater δ^{18} O, a freshwater flux was applied to the North Atlantic region between 61°W and 0° and 47°N–61°N (Supplementary Material, Fig. 9). As the ocean model's barotropic momentum equations are solved with a rigid lid approximation, surface freshwater fluxes are represented by fluxes of salt with a constant salt to freshwater mass ratio of 34.9 kg salt m^{-3}. The freshwater forcing time series is based on Menviel et al. (2015) where anomalous freshwater fluxes are optimized such that the simulated Heinrich Stadial temperature anomalies in the eastern subtropical North Atlantic best match the target alkenone-based sea surface temperature (SST) anomalies reconstructed from the Iberian Margin core MD01-2444 (Martrat et al., 2007). Here, this time series is extended to include HS3 and expanded to simulate smaller D-O stadials with smaller freshwater events.

The MIS3 period was characterized by long-term cooling, and an associated decrease in atmospheric CO_2 concentrations and growth in land ice volume. To take into account the accumulation of low δ^{18}O snow and ice on continents during MIS3, surface ocean $\delta^{18}O_w$ is artificially increased at a constant rate in the region north of 25°N throughout the simulations. This rate is consistent with a global mean $\delta^{18}O_w$ increase of 0.021‰ per 1000 years, based on the benthic LR04 stack of Lisiecki and Raymo (2005). The region north of 25°N was chosen as a broad approximation for potential source regions of water vapour involved in ice sheet accumulation. As the larger freshwater events lead to a shutdown of the AMOC, these events are followed by a freshwater withdrawal of −0.06 to −0.2 Sv (or the equivalent of an addition of 2 to $7 \cdot 10^6$ kg salt s^{-1}) in the same region as the freshwater hosing to trigger AMOC recovery. The salt flux triggering AMOC recovery does not carry an isotopic signature.

Three simulations were integrated: highFW, lowFW, and fwN (Table 1). The freshwater fluxes are identical during the highFW and fwN simulations, while the total volume of added freshwater is lower during the lowFW simulation. During the highFW and lowFW simulations, meltwater has a δ^{18} O ratio of −20‰, while meltwater does not carry an isotopic signature in the fwN simulation. Hence, ocean seawater δ^{18} O anomalies in the fwN simulation are solely due to changes in overturning circulation and resulting changes in climate patterns. By comparing highFW to fwN, we can estimate the impact of the addition and subsequent advection of δ^{18} O-depleted meltwater. Bagniewski et al. (2015) compared simulations of an idealized Heinrich event with paleo-proxy records of Heinrich stadials 1 and 4, and concluded that a meltwater

Table 1
Total volume of freshwater added to the North Atlantic during Heinrich stadials (HS5, HS4, and HS3), during a large D-O stadial (DO8) and during small D-O stadials (DO12 and DO11) in sea level equivalent (SLE) for the three simulations. During HS3 freshwater was added over two separate periods, here represented as a single event.

Experiment	SLE equivalent					Freshwater $\delta^{18}O$
	HS3	HS4	HS5	DO8	DO11,12	
highFW	3.5 m	10.5 m	7.9 m	4.2 m	2.2 m	−20‰
fwN	3.5 m	10.5 m	7.9 m	4.2 m	2.2 m	–
lowFW	3.2 m	4.6 m	3.7 m	2.6 m	2.2 m	−20‰

addition equivalent to 22 m of sea-level rise was too large. Hence, in our MIS3 transient simulations the volume of freshwater added to simulate Heinrich stadials is equivalent to ~ 7 m sea level rise (Table 1). The time series of the freshwater forcing applied to the North Atlantic during both highFW and lowFW simulations is shown in Fig. 1C.

2.3. Model–paleoproxy comparison

The simulated δ^{18} O of seawater ($\delta^{18}O_w$) reports the departure of the sample isotopic composition from the Standard Mean Ocean Water (Baertschi, 1976). Paleoproxy data record δ^{18} O of carbonate ($\delta^{18}O_c$), which measures the departure of the sample isotopic composition from the Pee Dee Belemnite standard (Craig, 1957). As carbonate precipitation from seawater is temperature-dependent, $\delta^{18}O_c$ also includes a temperature effect. Hence, to compare the model results with the paleoproxy $\delta^{18}O_c$ records we add a temperature effect to the simulated $\delta^{18}O_w$. Furthermore, $\delta^{18}O_w$ is calculated for proxy records which include both planktic $\delta^{18}O_c$ and SST data. For surface (planktic) $\delta^{18}O$ we use the equation derived by Shackleton (1974):

$$T = 16.9 - 4.38\left(\delta^{18}O_c - \delta^{18}O_w\right) + 0.10\left(\delta^{18}O_c - \delta^{18}O_w\right)^2$$

while for benthic $\delta^{18}O$ we use the equation derived by Marchitto et al. (2014):

$$T = \left(0.245 - \sqrt{0.045461 + 0.0044\left(\delta^{18}O_c - \delta^{18}O_w\right)}\right) \Big/ 0.0022$$

where T is the water temperature (°C).

The main modes of variability in major climate parameters (sea surface temperature (SST), surface atmospheric temperature (SAT), precipitation) and in their δ^{18} O signature (δ^{18} O precipitation, sea surface $\delta^{18}O_w$, sea surface $\delta^{18}O_c$) simulated for the MIS3 period have been determined with an Empirical Orthogonal Function (EOF) analysis. As δ^{18} O anomalies include a linear trend of 0.021‰ per 1000 years (please refer to Section 2.2 for details), the time series of δ^{18} O precipitation, sea surface $\delta^{18}O_w$ and sea surface $\delta^{18}O_c$ have been detrended prior to EOF analysis.

Model results are compared to paleoclimate records spanning MIS3 from 13 marine sediment cores in the North Atlantic (Supplementary Material, Fig. 9), as well as ice cores in Greenland (NGRIP, NGRIP Dating Group (2008)) and Antarctica (WAIS Divide Core, WAIS Divide Project Members (2015)). We focus our analysis on the Atlantic Ocean because $\delta^{18}O$ and SST anomalies in other ocean basins directly resulting from AMOC changes are smaller (Bagniewski et al., 2015) and could thus be influenced by other processes not represented here. The sediment cores were grouped into regions and depths (for benthic records) for which a similar stadial-interstadial $\delta^{18}O_c$ pattern can be expected. When multiple cores are present in one group, they are stacked into a single time series. All paleoproxy records from the North Atlantic are displayed on the GICC05 timescale. Simulated surface values are taken from the uppermost level of the ocean model (0–50 m depth).

3. Results

3.1. Circulation and ice core δ^{18} O response

Fig. 1A–D shows the evolution of the main forcing parameters and the resulting ocean circulation changes for the three transient experiments. As the only difference between simulations fwN and highFW is the δ^{18} O value of the meltwater forcing, the circulation changes simulated in fwN and highFW are the same. During Heinrich stadials as well as the D-O 8 stadial, the simulated AMOC shuts down and does not recover until an artificial salt flux is applied, whereas during D-O stadials 12 and 11, the AMOC weakens by about 30% and subsequently recovers once the meltwater forcing has stopped (Fig. 1D). A weakening of the AMOC leads to a decrease in Antarctic Bottom Water (AABW) formation by up to 20% during Heinrich events. During D-O stadials, changes in AABW lag the changes in AMOC by approximately 200–300 years. Despite significantly different freshwater flux rates during HS5, HS4, and DO8 for highFW and lowFW, circulation changes are similar for the two simulations, with AMOC shutdown taking about 300 years longer in lowFW.

Stadial conditions are characterized by cooler and drier conditions over Greenland, the North Atlantic and Europe (Supplementary Material, Fig. 10), causing a decrease in $\delta^{18}O$ of precipitation over these regions. As a result, $\delta^{18}O$ in snow precipitation over Greenland decreases during stadials (Fig. 1E). While the simulated $\delta^{18}O$ variations during Heinrich stadials are comparable to the $\delta^{18}O$ recorded in ice cores, the simulations underestimate the decrease during Dansgaard-Oeschger stadials (Fig. 1E). As observed in Antarctic ice cores, simulated Antarctic $\delta^{18}O$ is in anti-phase with Greenland during Heinrich stadials. However, only large events are simulated in Antarctica and the change in $\delta^{18}O$ during one of these large events (HS4) is underestimated (Fig. 1F). It has been suggested that enhanced AABW formation during Heinrich stadials could increase the poleward heat transport to high southern latitudes, thus leading to a greater warming of Antarctica (Meissner et al., 2008; Menviel et al., 2015). The weakening of AABW simulated here during Heinrich stadials (Fig. 1D) might thus explain the underestimated variability in Antarctic precipitation $\delta^{18}O$.

The simulated $\delta^{18}O$ anomalies in precipitation reproduce most of the millennial-scale variability, as well as the semi-linear trend in $\delta^{18}O$ for the entire MIS3 recorded in the Greenland core (Fig. 1E). The relatively small differences between highFW, fwN and lowFW experiments reflect the fact that in our simulations, $\delta^{18}O$ anomalies in precipitation are mostly due to temperature dependent fractionation.

3.2. Ocean $\delta^{18}O$ response at the surface

The time series and the corresponding spatial patterns of the EOF analysis for surface ocean variables are shown in Fig. 2. Not surprisingly, a pattern that closely follows changes in AMOC is the dominant EOF mode, explaining 58.14% of the variance in SST, 89.63% of the variance in $\delta^{18}O_w$, and 78.09% of the variance in $\delta^{18}O_c$.

Stadial conditions are characterized by cooling in the North Atlantic regions (Fig. 2A), as a weaker AMOC transports less warm, low-latitude water into the North Atlantic. Strongest amplitudes in SST changes are found near the North Atlantic Deep Water (NADW)

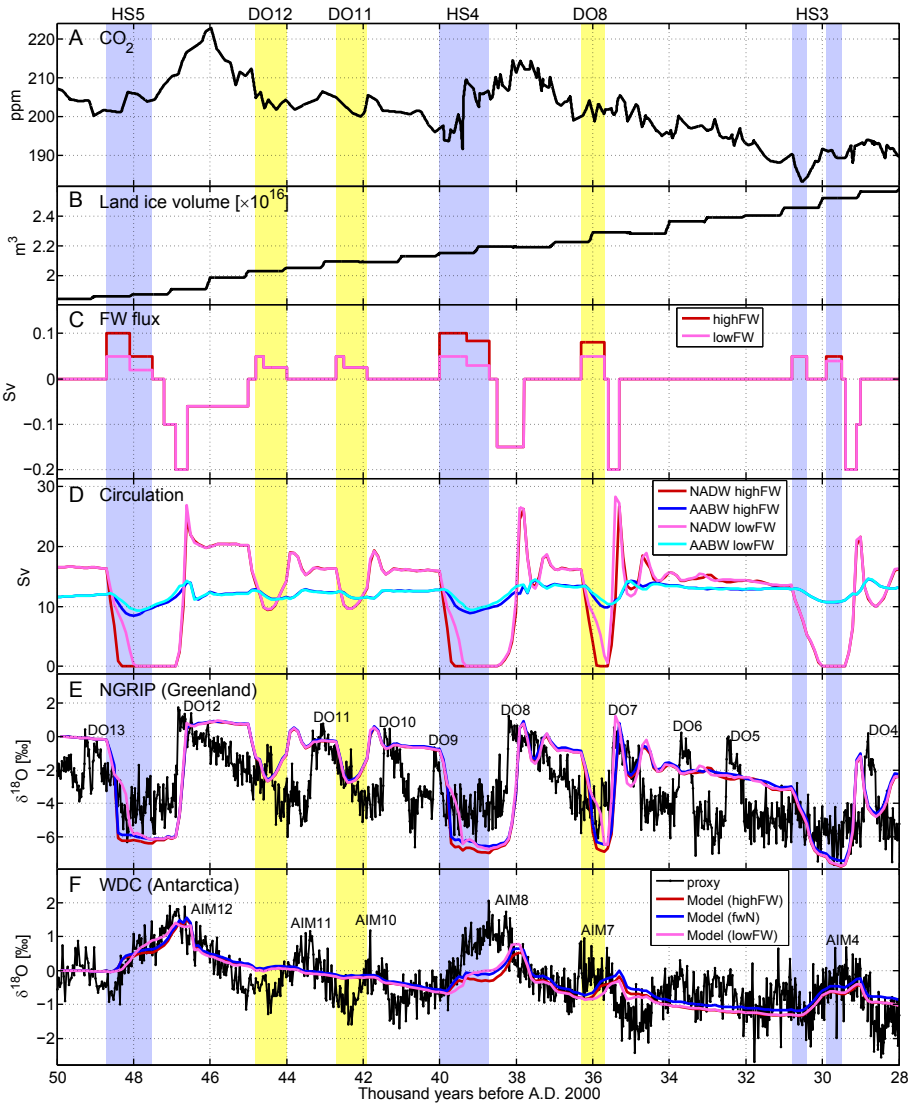

Fig. 1. Time series of the main forcing parameters (A–C) and the resulting changes in deep water circulation (D) and ice sheet $\delta^{18}O$ (E–F) for the three transient experiments. (A) Atmospheric CO_2 (ppm) (Bereiter et al., 2012; Ahn and Brook, 2014); (B) Land ice volume (m^3) (Abe-Ouchi et al., 2007); (C) Freshwater (FW) forcing (Sv); (D) Simulated North Atlantic Deep Water formation (NADW, red and pink) and Antarctic Bottom Water formation (AABW, blue and cyan) rates (Sv); (E) Simulated anomalies of $\delta^{18}O$ in snow precipitation over Greenland averaged between 28°W and 18°W, and 72°N – 77°N, superimposed by $\delta^{18}O$ anomalies from the NGRIP time series (NGRIP Dating Group, 2008); (F) Simulated anomalies of $\delta^{18}O$ in snow precipitation over Antarctica averaged between 116°W and 108°W, and 84°S – 76°S, superimposed by $\delta^{18}O$ anomalies from the WAIS Divide Core (WDC) time series (WAIS Divide Project Members, 2015). Red and blue represent highFW and fwN simulations; pink and cyan represent lowFW simulation; black represents forcing parameters and anomalies in paleoproxy records. Colored bars represent freshwater fluxes during Dansgaard-Oeschger (yellow) and Heinrich (blue) stadials. Dansgaard-Oeschger interstadials and Antarctic Isotope Maxima (AIM) are indicated above the time series (E and F). (For interpretation of the references to colour in this figure legend, the reader is referred to the web version of this article.)

formation sites, extending into a region southwest of Iceland (Fig. 2A). In response to the AMOC-driven temperature seesaw, sea surface warming is simulated in the subtropical South Atlantic and in parts of the Pacific Ocean.

Stadial conditions are further characterized by a decrease in sea surface $\delta^{18}O_w$ in the North Atlantic, and a decrease in sea surface $\delta^{18}O_c$ over the Atlantic and Southern Oceans (Fig. 2B and C). However, the strong response in North Atlantic SST to changes in AMOC reverses the sea surface $\delta^{18}O_c$ signal in the region southwest of Iceland (Fig. 2C).

While the corresponding principal component time series for SST is in very close agreement with changes in AMOC (Fig. 2D), this relationship is weaker for sea surface $\delta^{18}O_w$ and $\delta^{18}O_c$, where the anomalies associated with smaller meltwater events are disproportionately smaller. The differences in δ^{18} O response to large versus small meltwater events are analyzed in more detail in Section 3.4.

Fig. 3 and 4 show comparisons between the model results and reconstructed SST and planktic $\delta^{18}O_c$ from 13 marine sediment core records in the North Atlantic (Supplementary Material, Fig. 9). The simulated SST, $\delta^{18}O_w$ and $\delta^{18}O_c$ anomalies in the North Atlantic (Fig. 3A–C) follow the pattern seen in planktic records (MD95-2006, JPC13, SO82-5), i.e. a decrease in SST and $\delta^{18}O_w$ and an increase in $\delta^{18}O_c$ during stadials. The model is in particularly good agreement with SST and $\delta^{18}O_w$ anomalies during HS5, HS3, and DO8 from core SO82-5 (Fig. 3A and B, green lines), and during HS5 from core MD95-2006 (Fig. 3A and B, black lines). However, the model underestimates the anomalies observed during DO12 and DO11 in core MD95-2006, while the anomalies observed during the same events in the Irminger Sea (cores JPC13 and SO82-5 (thick

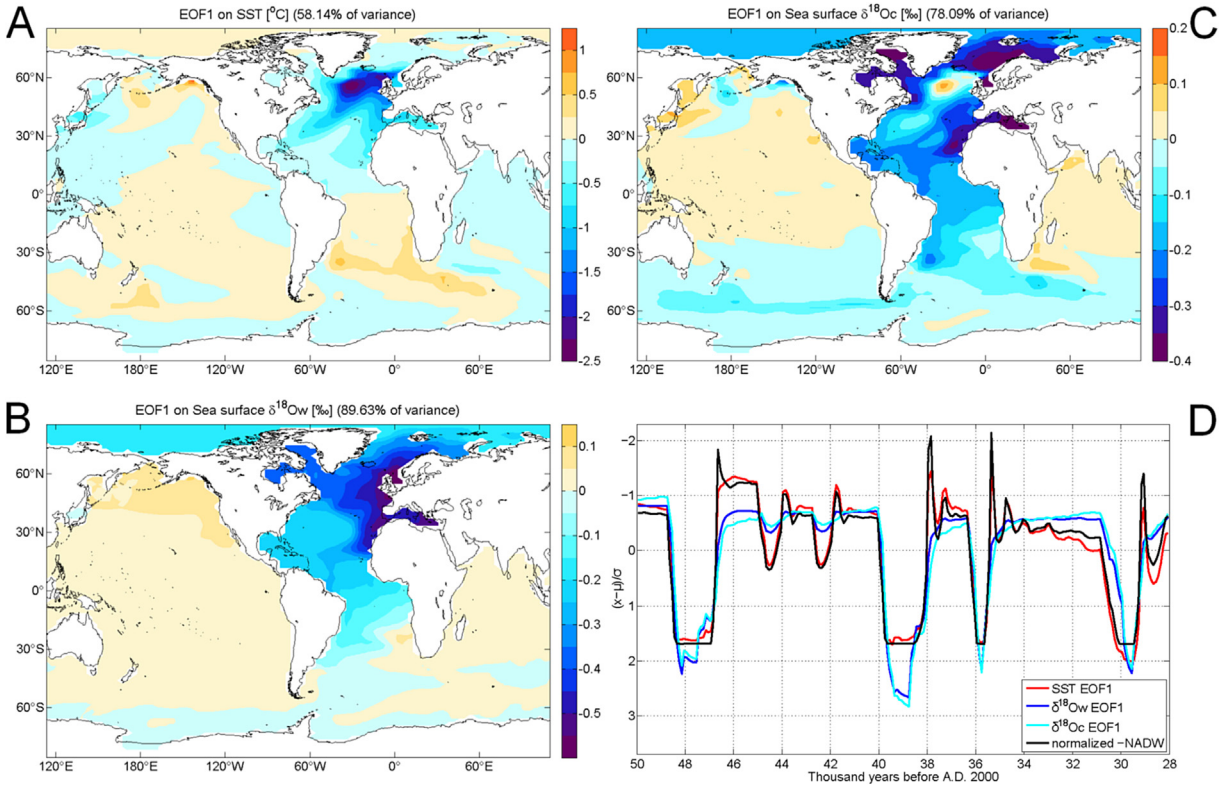

Fig. 2. (A) Pattern of first EOF of sea surface temperature (SST) anomalies (°C), which explains 58% of the variance; (B) Pattern of first EOF of detrended sea surface $\delta^{18}O_w$ anomalies (‰), which explains 90% of the variance; (C) Pattern of first EOF of detrended sea surface $\delta^{18}O_c$ anomalies (‰), which explains 78% of the variance; (D) normalized principal components of first EOFs of sea surface temperature (SST, red), sea surface $\delta^{18}O_w$ ($\delta^{18}O_w$, blue) and sea surface $\delta^{18}O_c$ ($\delta^{18}O_c$, cyan), and normalized North Atlantic Deep Water formation rate (NADW, black). Please note that the y axis and the normalized NADW time series in Fig. 2D have been reversed. (For interpretation of the references to colour in this figure legend, the reader is referred to the web version of this article.)

grey line in Fig. 3C) are of similar amplitude as in our simulations. The simulated $\delta^{18}O_w$ and $\delta^{18}O_c$ anomalies during Heinrich stadials are very different between the three simulations. For example, $\delta^{18}O_c$ decreases during HS5 and HS4 for the highFW simulation, but increases for the fwN and lowFW simulations (Fig. 3C).

In the Norwegian Sea (Fig. 3D), the simulated $\delta^{18}O_c$ anomalies are in relatively good agreement with the planktic record from core MD95-2010. In contrast to $\delta^{18}O_c$ anomalies at lower latitudes (Fig. 3A–C), there is a decrease during HS4, HS3 and DO8, and no significant change during DO12 and DO11. No significant $\delta^{18}O_c$ decrease is recorded during HS5 in the MD95-2010 core (Dokken and Jansen, 1999). The magnitudes of the simulated changes during HS4, HS3 and DO8 are in a good agreement with the proxy for simulation lowFW and are overestimated for simulation highFW.

SST anomalies at the Iberian Margin (Fig. 4A) are in good agreement with the alkenone-derived SST anomalies from MD01-2444 core (Martrat et al. (2007), green line). This was expected, as the Martrat et al. (2007) SST record was used as a tuning target when building the freshwater time series. However, the SST anomalies in cores MD99-2339 and MD95-2040, calculated using a modern analog technique, have much higher amplitudes (Fig. 4A, grey line). As a result, reconstructed $\delta^{18}O_w$ anomalies differ depending on the SST record used to calculate the temperature effect (grey and green lines in Fig. 4B). Observed $\delta^{18}O_c$ measured in Iberian margin sediment cores increases during each meltwater event, with higher amplitudes seen during larger events (Fig. 4C, grey line). In contrast, simulated $\delta^{18}O_c$ decreases during the large meltwater events. This discrepancy could be due to the simulated North Atlantic circulation. Indeed, reduced advection of low latitude high $\delta^{18}O$ waters when the AMOC is weak and the addition of depleted meltwater lead to greatest negative $\delta^{18}O_w$ anomalies along the western European coast (Fig. 2B). This effect might be overestimated at the Iberian Margin due to the coarse resolution of the model.

Finally, it is worth noting that all the Iberian Margin planktic $\delta^{18}O_c$ shown here are measured on surface dwelling *G. bulloides*, contrarily to northern North Atlantic $\delta^{18}O_c$, which are measured on surface to subsurface dwelling *N. pachyderma*. While phytoplankton blooms in the polar regions develop during summer months, temperate basins experience spring and autumn blooms.

3.3. Ocean $\delta^{18}O$ response at depth

Figs. 5 and 6 show a comparison between the model results and benthic $\delta^{18}O_c$ from 9 marine sediment core records in the North Atlantic at the location and depth of each core. The simulated benthic stadial-interstadial $\delta^{18}O_c$ anomalies are significantly different between different ocean depths. Between 1000 and 2000 m depth, the simulated anomaly during Heinrich stadials is negative in the northern North Atlantic (Fig. 5A and B) and positive at the Iberian Margin (Fig. 6A). This is followed by a negative spike in $\delta^{18}O_c$ at the end of the stadial that propagates through all depths levels and is most prominent in the time series below 3000 m (Figs. 5D and 6C), caused by the recovery of AMOC (Bagniewski et al., 2015). Anomalies during smaller stadials are generally small, with a decrease in $\delta^{18}O_c$ at intermediate depth at the Iberian Margin (Fig. 6A) and below 2000 m in the northern North Atlantic (Fig. 6C and D). These patterns are overall in good agreement with the sediment records, particularly for cores MD95-2010 (Fig. 5A) and MD95-2339 (Fig. 6A), although HS3 is not recorded in MD95-

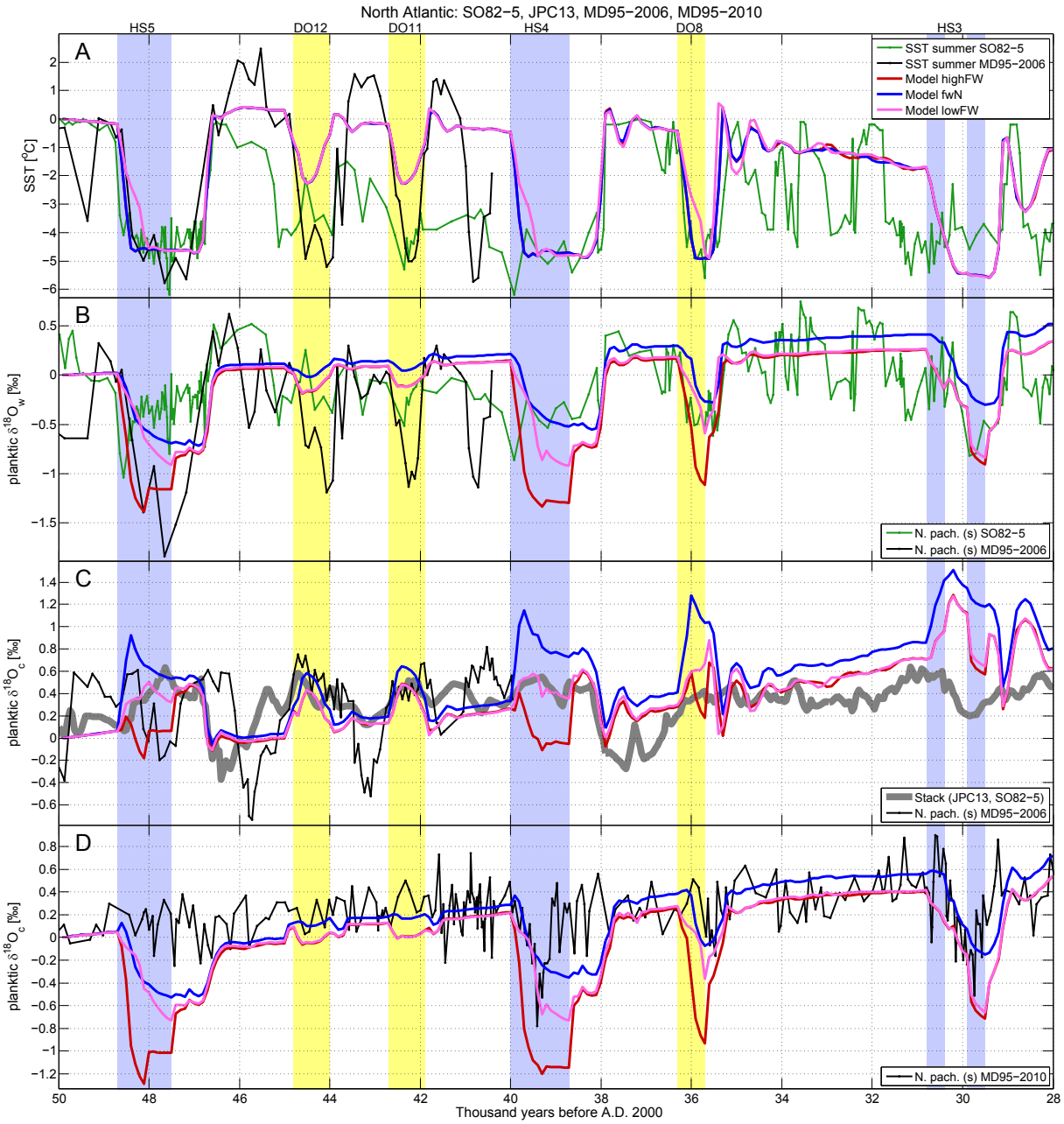

Fig. 3. SST (A), $\delta^{18}O_w$ (B), and $\delta^{18}O_c$ (C–D) anomalies simulated in experiments highFW (red), fwN (blue) and lowFW (pink), compared to planktic foraminiferal anomalies for cores JPC13 (Hodell et al., 2010), SO82-5 (van Kreveld et al., 2000), MD95-2006 (Dickson et al., 2008) and MD95-2010 (Dokken and Jansen, 1999). The thick grey line represents a stack of $\delta^{18}O_c$ anomalies from cores JPC13 and SO82-5. Paleoproxy records are all from *Neogloboquadrina pachyderma* foraminifera and have been shifted in time and plotted on the GICC05 timescale used by the model. Colored bars represent freshwater fluxes during Dansgaard-Oeschger (yellow) and Heinrich (blue) stadials. (For interpretation of the references to colour in this figure legend, the reader is referred to the web version of this article.)

2339. The three simulations show very different results in the North Atlantic at 2000–3000 m depth (Fig. 5C).

3.4. Difference between Heinrich and Dansgaard-Oeschger stadials

The simulated $\delta^{18}O_c$ anomalies are separated into changes due to meltwater input, circulation and climate effects as well as temperature (Figs. 7 and 8, Bagniewski et al. (2015)). As the added meltwater has no isotopic signature in fwN, $\delta^{18}O_w$ anomalies in the fwN simulation are solely representing the impact of changes in circulation and climate ("circulation and climate" effect). The impact of the ^{18}O-depleted meltwater addition ("meltwater effect") is obtained by comparing the anomalies in highFW with respect to fwN. Finally, the impact of temperature on $\delta^{18}O_c$ anomalies is calculated using the fractionation equations of Shackleton (1974) (for planktic foraminifera) and Marchitto et al. (2014). As mentioned in Section 2.2, ocean $\delta^{18}O$ was artificially increased at a constant rate of 0.021‰ per 1000 years. Thus, a linear increase in $\delta^{18}O$ occurs throughout both highFW and fwN simulations. This increase can be seen in $\delta^{18}O_c$ (highFW) (Fig. 7A and B) and in the "circulation and climate" signal (fwN) (Fig. 7C and D). However, it should not be interpreted as a "circulation and climate" signal as it is not caused by ocean dynamics. It may rather be interpreted as representing the background signal of land ice growth.

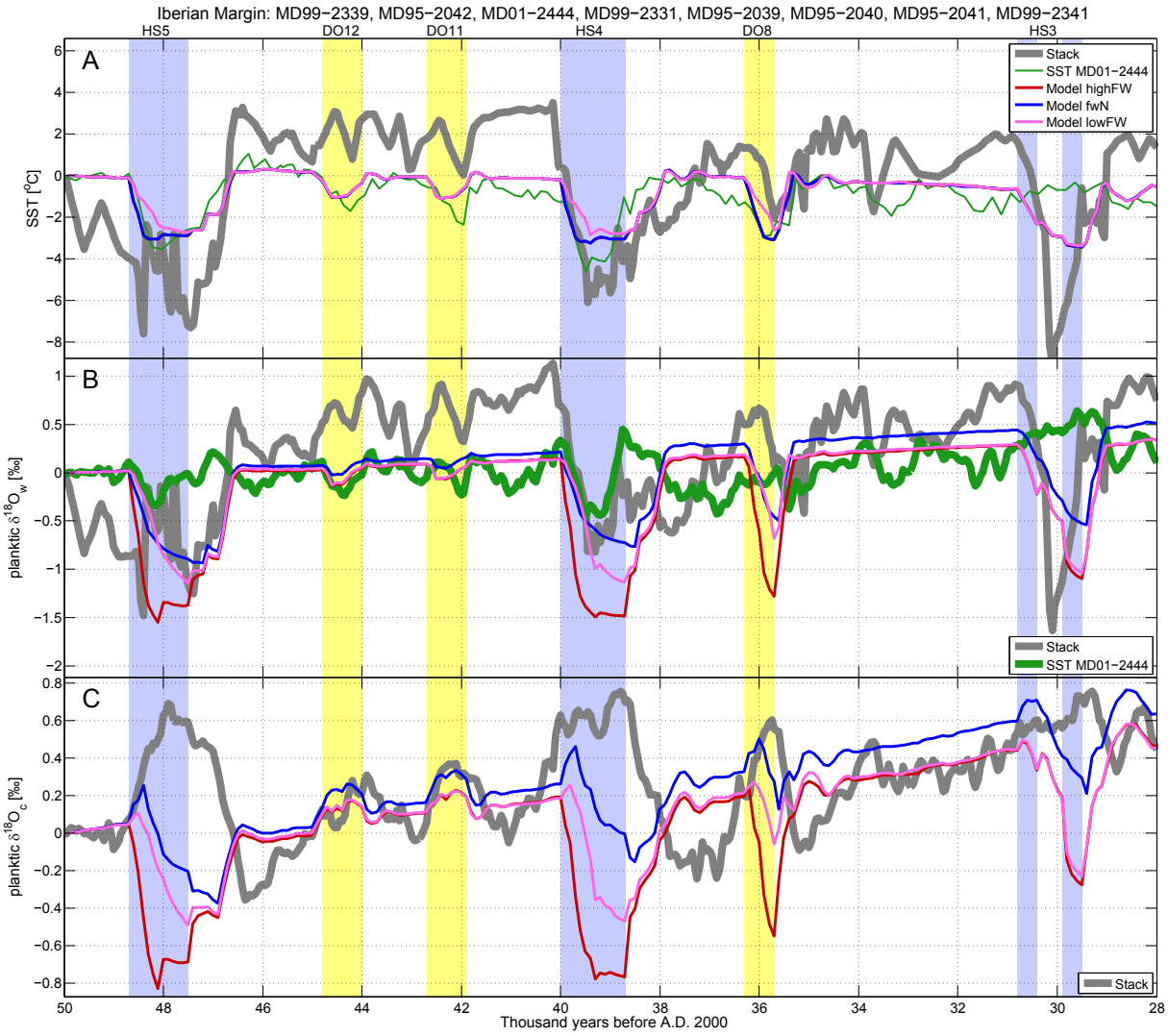

Fig. 4. SST (A), $\delta^{18}O_w$ (B), and $\delta^{18}O_c$ (C) anomalies simulated in experiments highFW (red), fwN (blue) and lowFW (pink), compared to planktic foraminiferal anomalies. The thick grey line represents a stack of SST anomalies (A) from cores MD99-2339 (Voelker et al., 2006) and MD95-2040 (Voelker and de Abreu, 2011); stacks of $\delta^{18}O_w$ (B) and $\delta^{18}O_c$ (C) anomalies from cores MD99-2339 (Voelker et al., 2006), MD95-2042 (Eynaud et al., 2009), MD01-2444 (Hodell et al., 2013), MD99-2331 (Eynaud et al., 2009), MD95-2039 (Eynaud et al., 2009), MD95-2040 (Voelker and de Abreu, 2011), MD95-2041 (Eynaud et al., 2009), and MD99-2341 (Eynaud et al., 2009). The thick green line (B) represents the stack of $\delta^{18}O_w$ anomalies from cores MD99-2339, MD95-2042, MD01-2444, MD99-2331, MD95-2039, MD95-2040, MD95-2041, and MD99-2341 calculated based on MD01-2444 (Martrat et al., 2007) SST data. Paleoproxy records are all from *Globigerina bulloides* foraminifera and have been shifted in time and plotted on the GICC05 timescale used by the model. Colored bars represent freshwater fluxes during Dansgaard-Oeschger (yellow) and Heinrich (blue) stadials. (For interpretation of the references to colour in this figure legend, the reader is referred to the web version of this article.)

Heinrich-induced anomalies (Figs. 7 and 8A–D) have a global impact on $\delta^{18}O_c$. While largest anomalies are simulated in the North Atlantic, significant changes extend into the North Pacific and the Southern Ocean. Reduced meridional transport of high $\delta^{18}O$ water to the North Atlantic (Fig. 8B) in addition to fluxes of low $\delta^{18}O$ meltwater (Fig. 8C) lead to significant (up to 1.2‰, Fig. 8A) negative $\delta^{18}O_c$ anomalies in the surface North Atlantic. A simultaneous decrease in SST offsets part of this anomaly through a positive "temperature effect" on $\delta^{18}O_c$ (Figs. 7G and 8D).

In contrast, the impact of smaller freshwater events, such as DO11 (Fig. 8E–H), on $\delta^{18}O_c$ is mostly limited to a subpolar North Atlantic region southwest of Iceland. The local $\delta^{18}O_c$ increase (Fig. 8E) develops as strong cooling induces a positive "temperature effect" on $\delta^{18}O_c$ (Fig. 7G). Since AMOC is weakened but does not shut down, the surface "circulation and climate" signal is negligible (Figs. 8F and 7C), and the "meltwater signal" is significantly weaker than during Heinrich stadials (Figs. 8G and 7E) as a result of both lower flux rates and the fact that the meltwater is continuously convected and advected into the deep ocean through formation of NADW.

As a result of the strong cooling in the region southwest of Iceland, sea surface $\delta^{18}O_c$ increases in this region during both Heinrich and D-O stadials (Fig. 8A and E). This anomaly corresponds to the cooling pattern simulated in response to a reduction in the AMOC (Stouffer et al., 2006). It is also consistent with the exceptional twentieth-century cooling observed in the same area, which has been suggested to be caused by a weakening of the AMOC (Rahmstorf et al., 2015). Due to a lower magnitude of $\delta^{18}O_w$ depletion in the North Atlantic during a D-O stadial (Fig. 8F and G) than during a Heinrich Stadial (Fig. 8B and C), the resulting increase in $\delta^{18}O_c$ southwest of Iceland is greater during DO11 (up to 1‰) than during HS5 (up to 0.5‰).

In the surface South Atlantic, moderate $\delta^{18}O_c$ anomalies are simulated during Heinrich stadials, whereas during D-O stadials

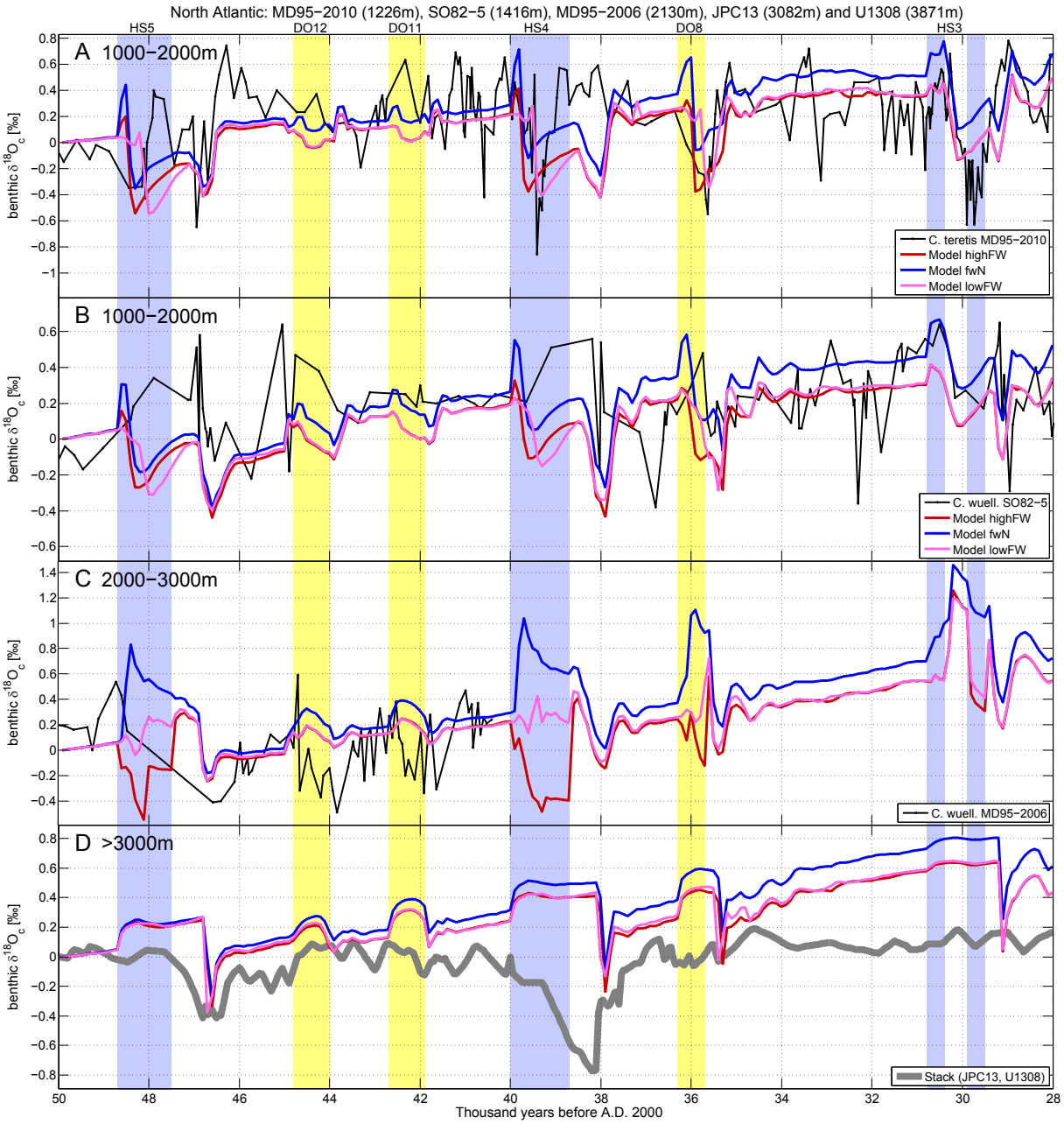

Fig. 5. Intermediate and deep ocean $\delta^{18}O_c$ anomalies simulated in experiments highFW (red), fwN (blue) and lowFW (pink), compared to benthic foraminiferal anomalies for cores (A) MD95-2010 (Dokken and Jansen, 1999) located at 1226 m depth; (B) SO82-5 (van Kreveld et al., 2000) located at 1416 m depth; (C) MD95-2006 (Dickson et al., 2008) located at 2130 m depth; (D) JPC13 (Hodell et al., 2010) and U1308 (Hodell et al., 2008) located at 3082 m and 3871 m depth, respectively. The thick grey line represents a stack of $\delta^{18}O_c$ anomalies from deep North Atlantic cores JPC13 and U1308. Paleoproxy records have been shifted in time and plotted on the GICC05 timescale used by the model. Colored bars represent freshwater fluxes during Dansgaard-Oeschger (yellow) and Heinrich (blue) stadials. (For interpretation of the references to colour in this figure legend, the reader is referred to the web version of this article.)

the $\delta^{18}O_c$ anomalies are negligible (Fig. 7A). $\delta^{18}O_c$ in the Southern Ocean decreases by up to 0.4‰ during a large freshwater event (Fig. 8A), due to both a negative meltwater signal (Fig. 8C), and a positive SST anomaly (Fig. 8D) caused by weaker northward water transport in the Atlantic Ocean.

Deep ocean $\delta^{18}O_c$ anomalies (Fig. 7B) are mostly driven by the "temperature effect" (Fig. 7H). Deep ocean $\delta^{18}O_c$ increases by up to 0.15‰ in the North Atlantic during freshwater events. During the AMOC resumption, $\delta^{18}O_c$ rapidly decreases by as much as 0.6‰ and subsequently recovers. The AMOC resumption $\delta^{18}O_c$ signal is significantly weaker after a small freshwater event.

4. Discussion

To our knowledge, these are the first transient simulations of Marine Isotope Stage 3 integrated with an oxygen isotope enabled model. These simulations allow us to conduct EOF analyses of millennial scale variability, discuss differences between Heinrich and D-O stadials, and directly compare time series of simulated $\delta^{18}O$ anomalies with ice core and sediment data.

EOF decompositions of the main climate variables and their $\delta^{18}O$ signature indicate that most of the simulated MIS3 variability can be explained by AMOC changes (Fig. 2, Supplementary Material

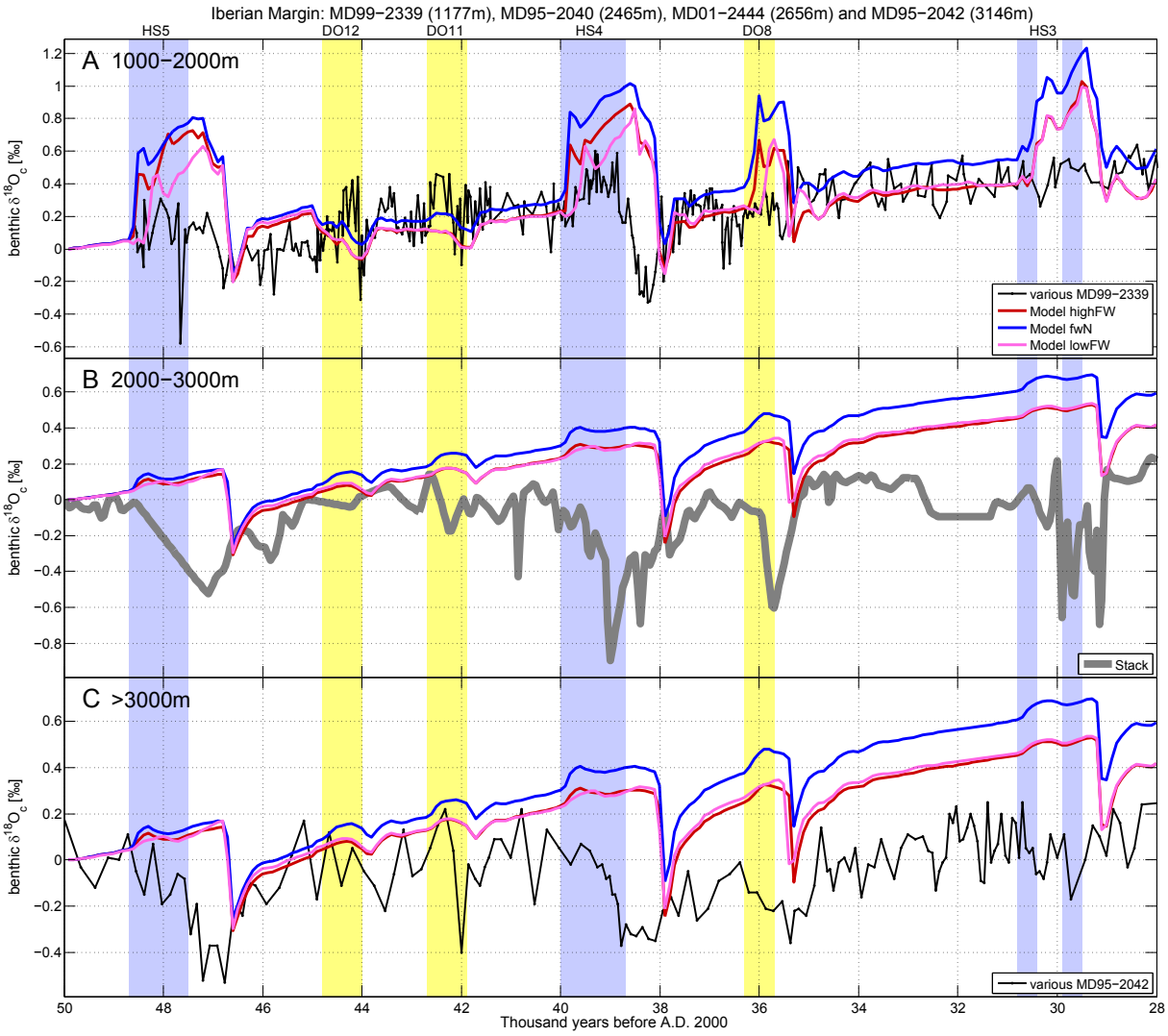

Fig. 6. Intermediate and deep ocean $\delta^{18}O_c$ anomalies simulated in experiments highFW (red), fwN (blue) and lowFW (pink), compared to benthic foraminiferal anomalies for cores (A) MD99-2339 (Voelker et al., 2006) located at 1177 m depth; (B) MD95-2040 (Voelker and de Abreu, 2011) and MD01-2444 (Hodell et al., 2013) located at 2465 m and 2656 m depth, respectively; (C) MD95-2042 (Shackleton et al., 2000) located at 3146 m depth. The thick grey line represents a stack of $\delta^{18}O_c$ anomalies from cores MD95-2040 and MD01-2444. Paleoproxy records have been shifted in time and plotted on the GICC05 timescale used by the model. Colored bars represent freshwater fluxes during Dansgaard-Oeschger (yellow) and Heinrich (blue) stadials. (For interpretation of the references to colour in this figure legend, the reader is referred to the web version of this article.)

Fig. 10). Weak AMOC is associated with a decrease in SST, precipitation, $\delta^{18}O$ precipitation, and surface $\delta^{18}O_w$ in the North Atlantic.

As sea-level decreases by ~ 20 m across MIS3 due to continental ice-sheet growth, the mean oceanic $\delta^{18}O$ increases by ~ 0.5‰, in agreement with the long-term trend observed in marine sediment cores (Figs. 3–6). On the other hand, as conditions get generally cooler, Antarctic and Greenland ice cores display a long-term $\delta^{18}O$ decrease, which is in good agreement with the simulated negative trends (Fig. 1E and F). To simulate variability on millennial timescales, we impose meltwater fluxes equivalent to a mean sea-level increase of about 7 m during Heinrich stadials and 2–4 m during smaller stadials (Table 1). The magnitudes of these imposed fluxes are on the lower bound of estimates for sea-level changes during Heinrich events (Siddall et al., 2008). Given that our isotopic signature of meltwater (−20‰) is also a conservative estimate (Hillaire-Marcel and de Vernal, 2008), a larger meltwater input (and thus sea-level increase) and/or more depleted signature of meltwater (e.g., −30‰) would lead to a greater amplitude of negative $\delta^{18}O$ anomalies at the surface of the North Atlantic, which would be difficult to reconcile with $\delta^{18}O_c$ measured in marine sediment cores.

The simulations are in a relatively good agreement with $\delta^{18}O$ signals from ice cores in Greenland and Antarctica (Fig. 1E and F). All Dansgaard-Oeschger stadials are identifiable in the simulated Greenland precipitation $\delta^{18}O$, except for DO10, DO7, and DO6, which were not included in the experimental setup. However, the model does not reproduce Antarctic Isotope Maxima 11 and 10 (corresponding to DO12 and DO11 stadials), and underestimates the anomalies during AIM8 (corresponding to HS4). As discussed in Menviel et al. (2015), this could be due to insufficient (up to 1 °C) simulated warming over Antarctica and the Southern Ocean, where paleoproxy records suggest a ~ 2 °C warming (e.g. Pahnke and Zahn, 2005; Jouzel et al., 2007; Caniupán et al., 2011). Stronger AABW transport in response to weakened AMOC during Heinrich stadials would enhance the warming over Antarctica and the Southern Ocean, leading to a better agreement with paleoproxy records (Menviel et al., 2015). In our simulations, AABW weakens during stadials, hence meridional heat transport is too small to generate a

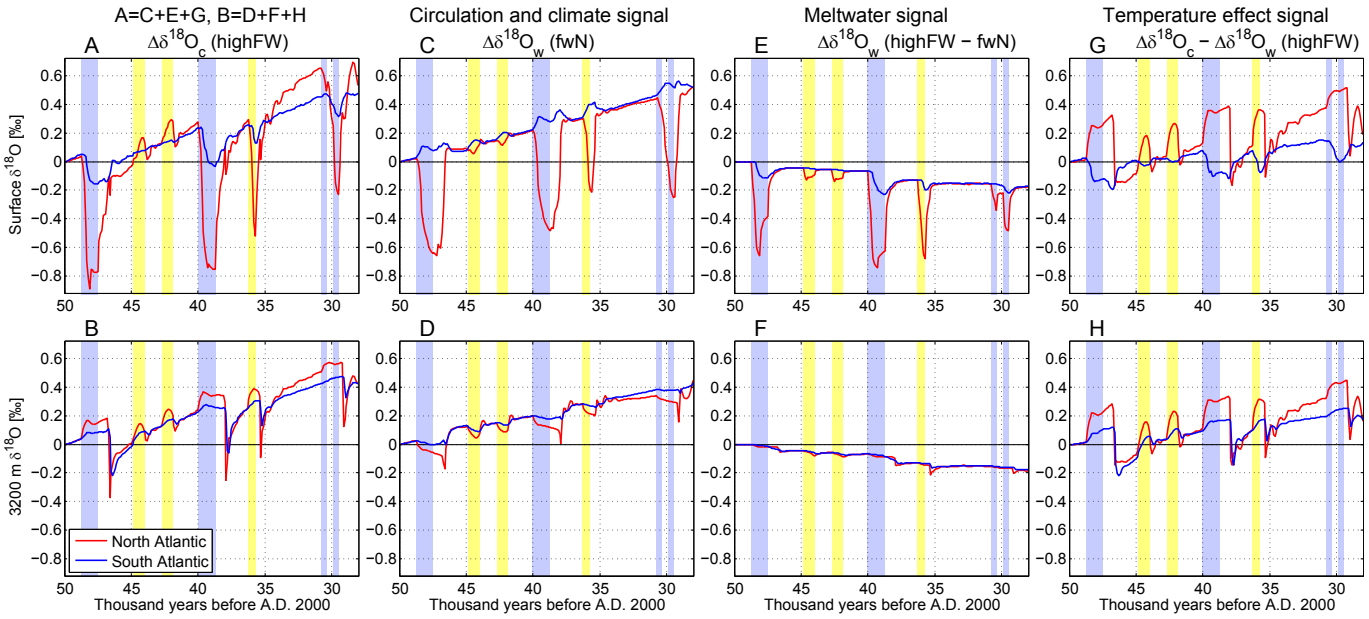

Fig. 7. Average $\delta^{18}O$ anomalies (‰) in the North Atlantic (red line) between 30°N and 60°N and the South Atlantic (blue line) between 60°S and 30°S at the surface (top) and at 3200 m depth (bottom). (A and B) $\delta^{18}O_c$ anomalies for experiment highFW; (C and D) $\delta^{18}O_w$ anomalies for experiment fwN; (E and F) difference between $\delta^{18}O_w$ (highFW) and $\delta^{18}O_w$ (fwN), representing the meltwater signal; (G and H) difference between $\delta^{18}O_c$ (highFW) and $\delta^{18}O_w$ (highFW), representing the temperature effect. Colored bars represent freshwater fluxes during Dansgaard-Oeschger (yellow) and Heinrich (blue) stadials. (For interpretation of the references to colour in this figure legend, the reader is referred to the web version of this article.)

strong enough North Atlantic–South Atlantic seesaw response.

The effect of meltwater input on North Atlantic $\delta^{18}O_c$ strongly depends on the flux rate and on the isotopic ratio of the meltwater. Our simulations suggest that surface North Atlantic $\delta^{18}O_c$ decreases during Heinrich stadials, because the signal is dominated by meltwater, as well as circulation and climate contributions. However, North Atlantic $\delta^{18}O_c$ increases during weaker stadials, when the temperature effect accounts for the largest fraction of the anomaly (Fig. 7A). The difference is particularly strong close to deep water formation sites (Figs. 3C and 5C), where both surface and deep water $\delta^{18}O_c$ can either increase or decrease depending on the flux rate and the isotopic ratio of the meltwater. Arguably, this is supported by the MD95-2006 record (Fig. 3C), where planktic $\delta^{18}O_c$ decreases during HS5 and increases during the two following D-O stadials.

The strong North Atlantic SST decrease in response to AMOC weakening may therefore reverse the negative $\delta^{18}O_c$ signal in the region south of Iceland (Fig. 2). This subpolar cooling in the North Atlantic region south of Iceland appears to be a robust feature of AMOC weakening (Stouffer et al., 2006; Rahmstorf et al., 2015). We therefore anticipate that further studies of this region would greatly improve the understanding of past changes in AMOC. Changes in sea surface $\delta^{18}O_w$ in the South Atlantic, South Pacific and Indian Ocean are small in our study (Fig. 7), therefore $\delta^{18}O_c$ anomalies in these regions are mostly due to changes in ocean temperature.

While simulated surface $\delta^{18}O_c$ are generally in a good agreement with planktic $\delta^{18}O_c$ from North Atlantic sediment cores, the simulated decrease in surface $\delta^{18}O_c$ off the Iberian Margin is at odds with the increase in planktic $\delta^{18}O_c$ recorded during Heinrich stadials. One possible reason for this discrepancy might be the fact that the simulated temperature decrease is too small to overcome the strong $\delta^{18}O_w$ decrease. The simulated 3 °C SST decrease agrees with the alkenone-derived SST of core MD01-2444, however it is weaker than the anomalies obtained using the modern analog technique (cores MD99-2339 and MD95-2040, Fig. 4A) and weaker than the 5 °C decrease simulated for the Irminger Sea (SO82-5, Fig. 3A). The model might also overestimate the $\delta^{18}O_w$ anomalies in the Mediterranean Sea and along the eastern North Atlantic coast during large stadials due to its coarse resolution (Spence et al., 2013). As seen in Fig. 8B and C, the changes in oceanic circulation as well as the addition of depleted meltwater lead to relatively large negative $\delta^{18}O_w$ anomalies concentrated off the Iberian Margin and in the Mediterranean Sea in the model simulation.

The paleo records reproduced in Fig. 3 are based on $\delta^{18}O_c$ measurements of a small planktonic foraminifera, *N. pachyderma*. *N. pachyderma* is the dominant species in polar waters nowadays (Kucera, 2007). It is a surface to subsurface dwelling species whose highest flux rates are observed during, or shortly after, summer blooms. The $\delta^{18}O_c$ of this species has been shown to follow SST variability over a wide range of latitudes and hydrographic conditions (Charles and Fairbanks, 1990). However, in some instances, departures from isotopic equilibrium with ambient Arctic waters have been observed (van Donk and Mathieu, 1969; Kohfeld et al., 1996; Bauch et al., 1997).

While the records of *N. pachyderma* most likely reflect surface to subsurface summer temperatures, the omnivorous and surface dwelling *G. bulloides* (Fig. 4) likely experienced spring and autumn blooms. Furthermore, *G. bulloides* might not record the full range of SST changes during MIS 3. For example, Bard et al. (1989) analyzed two cores off Portugal and found that the $\delta^{18}O_c$ recorded by *G. bulloides* only followed the expected trend of the temperature effect between 0.4 and 2.2‰ during the Holocene. The measured $\delta^{18}O_c$ values were nearly constant outside this range, suggesting seasonal or subsurface growth and calcification. The discrepancy between *N. pachyderma* records which mostly show a decrease in their $\delta^{18}O_c$ values during Heinrich events and D-O stadials in the northern North Atlantic (Fig. 3, Cortijo et al., 1997) and *G. bulloides* records which mostly show an increase (Fig. 4, Hodell et al., 2013), might therefore also be due to the species-specific ecology, the seasonality and depth of calcification in the water column.

In North Atlantic intermediate water masses, $\delta^{18}O_w$ decreases

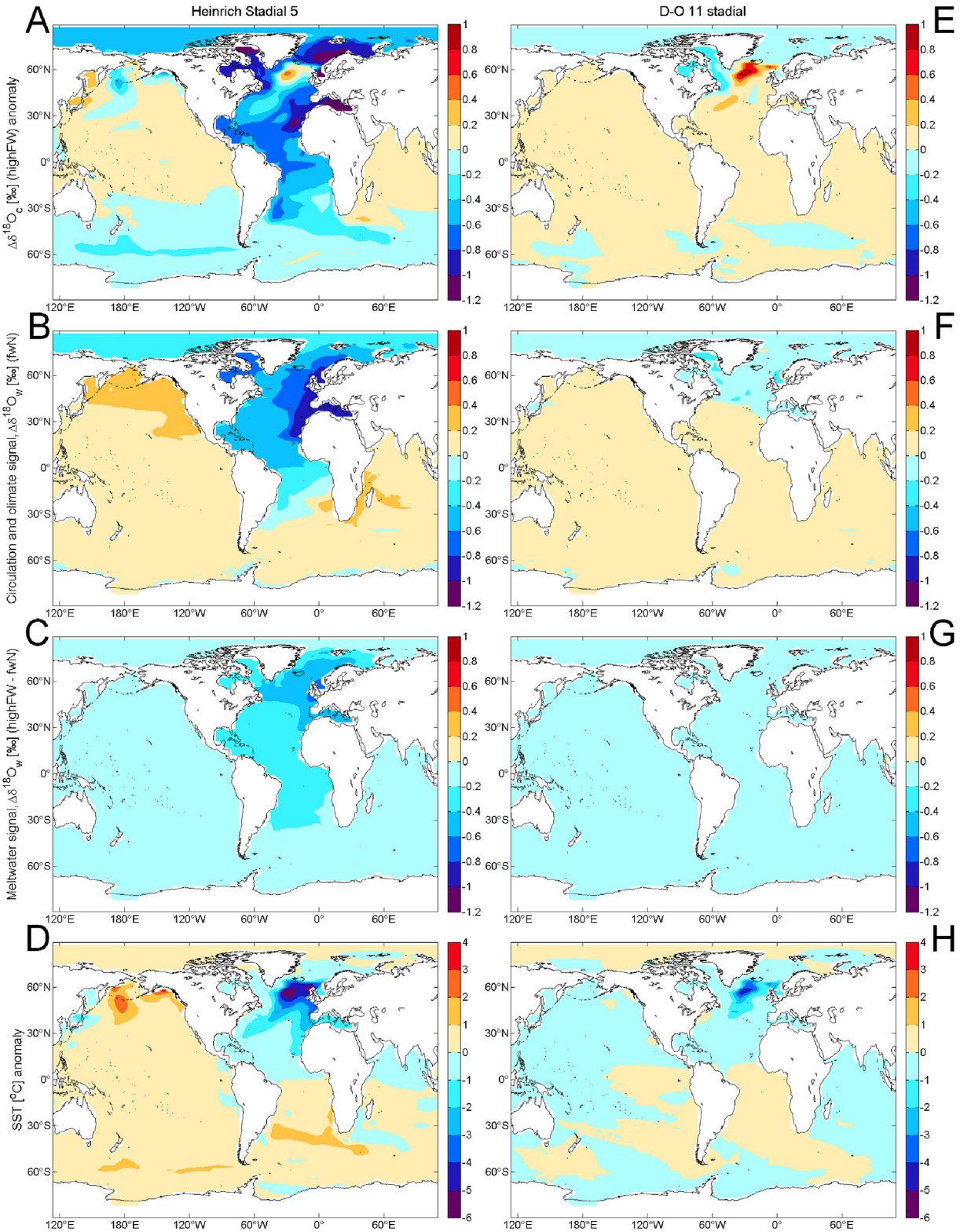

Fig. 8. Sea surface anomalies simulated during Heinrich Stadial 5 (left) and Dansgaard-Oeschger stadial 11 (right). (A and E) $\delta^{18}O_c$ (‰) anomalies for experiment highFW; (B and F) $\delta^{18}O_w$ anomalies (‰) for experiment fwN; (C and G) difference between $\delta^{18}O_w$ (highFW) and $\delta^{18}O_w$ (fwN), representing the meltwater signal; (D and H) temperature anomalies (°C).

by ~ 0.2–0.4‰ due to the advection of negative $\delta^{18}O_w$ anomalies from the surface of the North Atlantic (Fig. 5A and B). The North Atlantic cooling also spreads to intermediate layers, and in some regions offsets the $\delta^{18}O_w$ decrease as can be seen in core MD99-2339 (Fig. 6A), even though in our simulations the cooling might be overestimated (Bagniewski et al., 2015). Intermediate depth

temperature changes in the North Atlantic during a weakening of the AMOC are complex, as they reflect the competing effects of surface cooling and subsurface warming (Brady and Otto-Bliesner, 2011; Bagniewski et al., 2015).

Benthic $\delta^{18}O_c$ records below 2000 m in the North Atlantic generally display a decrease during stadials and particularly during Heinrich stadials. This was interpreted as indicating a warming of deep waters (Margari et al., 2010). In our simulations the simulated $\delta^{18}O_c$ in the deep North Atlantic does not vary much (Figs. 5C and D, 6B and C) as a result of the compensating effects of decreased $\delta^{18}O_w$ and lower ocean temperatures (Fig. 7). This disagreement between model and proxy could be due to a misrepresentation of changes in AABW during Heinrich stadials. The simulated negative $\delta^{18}O_c$ peak in the deep ocean, identified in Bagniewski et al. (2015) as a signal of AMOC recovery, is a solid feature in most North Atlantic records at different depths (Figs. 5 and 6) and has been discussed in previous studies (e.g. Rasmussen et al., 1996; Rasmussen and Thomsen, 2004; Dokken and Jansen, 1999; van Kreveld et al., 2000; Hillaire-Marcel and de Vernal, 2008; Meland et al., 2008).

Since changes in $\delta^{18}O_c$ variations can be caused by a combination of factors, including meltwater from icebergs, river discharge, changes in oceanic circulation, precipitation and/or evaporation, sea ice formation and melting as well as temperature changes, simulating $\delta^{18}O_c$ variations represents a real challenge to the modelling community. Precise model-data comparisons of high resolution $\delta^{18}O_c$ records and high resolution simulations can therefore provide important information on the respective drivers and impacts of millennial-scale changes of the last glacial period. This represents a future challenge for both the paleoproxy and modelling communities.

5. Conclusions

The relatively good agreement between freshwater-driven anomalies in our simulations and millennial-scale variability in paleoproxy ice and sediment records presents strong evidence for the link between stadial-interstadial variability, changes in the Atlantic Meridional Overturning Circulation (AMOC) and continental ice-sheet instabilities. The comparison between simulated $\delta^{18}O$ and paleoproxy records supports an AMOC shutdown during Heinrich stadials and a 30–50% weakening of the AMOC during Dansgaard-Oeschger stadials, in agreement with previous studies (e.g. Sarnthein et al., 2001; Ganopolski and Rahmstorf, 2001; Menviel et al., 2014).

We find a significant difference in simulated $\delta^{18}O_c$ anomalies between Heinrich and D-O stadials. This is mainly due to the weaker transport of low latitude, ^{18}O enriched, surface waters to the North Atlantic as well as the larger volume of ^{18}O depleted meltwater involved during Heinrich stadials. In a large region south of Iceland, the temperature effect becomes dominant during smaller events and causes the simulated changes in surface $\delta^{18}O_c$ during large versus small stadials to be of opposite sign. A similar pattern can be seen in core MD95-2006 (Fig. 3C).

The general agreement between simulated and observed $\delta^{18}O_c$ from the northern North Atlantic points to a sea-level rise equivalent to 4–11 m during Heinrich stadials. As the meltwater signal plays a major role in shaping $\delta^{18}O_c$ anomalies only during Heinrich stadials (Fig. 7E), it cannot be ruled out by our results that AMOC weakening during D-O stadials was driven by mechanisms other than land ice discharge. It is also plausible that the iceberg discharge was driven by internal ocean dynamics operating on millennial timescales (Flückiger et al., 2006; Ahn and Brook, 2008; Meissner et al., 2008; Marcott et al., 2011). For example, the Southern Ocean has been put forward as a likely candidate (Meissner et al., 2008). Additional high resolution planktic $\delta^{18}O$ records from the North Atlantic and Southern Ocean covering the last glacial period are needed to better pinpoint the mechanisms leading to Heinrich and D-O stadials.

Acknowledgements

We thank an anonymous reviewer and the Editor, Henning A. Bauch, for providing constructive suggestions on an earlier version of this manuscript. This study was funded by the Australian Research Council (DE150100107) and supported by an award under the Merit Allocation Scheme on the NCI National Facility at the Australian National University. WB is grateful for a UNSW Tuition Fee Scholarship. KJM acknowledges support from UNSW Gold- and Silverstar awards.

Appendix A. Supplementary data

Supplementary data related to this article can be found at http://dx.doi.org/10.1016/j.quascirev.2017.01.007.

References

Abe-Ouchi, A., Segawa, T., Saito, F., 2007. Climatic conditions for modelling the Northern Hemisphere ice sheets throughout the ice age cycle. Clim. Past 3, 423–438.
Ahn, J., Brook, E.J., 2008. Atmospheric CO_2 and climate on millennial time scales during the last glacial period. Science 322, 83–85.
Ahn, J., Brook, E.J., 2014. Siple Dome ice reveals two modes of millennial CO_2 change during the last ice age. Nat. Commun. 5.
Álvarez-Solas, J., Robinson, A., Montoya, M., Ritz, C., 2013. Iceberg discharges of the last glacial period driven by oceanic circulation changes. Proc. Natl. Acad. Sci. 110, 16350–16354.
Archer, D., 1996. A data-driven model of the global calcite lysocline. Glob. Biogeochem. Cycles 10, 511–526.
Baertschi, P., 1976. Absolute ^{18}O content of standard mean ocean water. Earth Planet. Sci. Lett. 31, 341–344.
Bagniewski, W., Meissner, K.J., Menviel, L., Brennan, C.E., 2015. Quantification of factors impacting seawater and calcite $\delta^{18}O$ during Heinrich Stadials 1 and 4. Paleoceanography 30, 895–911.
Bard, E., Fairbanks, R., Arnold, M., Maurice, P., Duprat, J., Moyes, J., Duplessy, J.-C., 1989. Sea-level estimates during the last deglaciation based on $\delta^{18}O$ and accelerator mass spectrometry ^{14}C ages measured in Globigerina bulloides. Quat. Res. 31, 381–391.
Barron, E., Pollard, D., 2002. High-resolution climate simulations of oxygen isotope stage 3 in Europe. Quat. Res. 58, 296–309.
Bauch, D., Carstens, J., Wefer, G., 1997. Oxygen isotope composition of living Neogloboquadrina pachyderma (sin.) in the Arctic Ocean. Earth Planet. Sci. Lett. 146, 47–58.
Bereiter, B., Lüthi, D., Siegrist, M., Schüpbach, S., Stocker, T.F., Fischer, H., 2012. Mode change of millennial CO_2 variability during the last glacial cycle associated with a bipolar marine carbon seesaw. Proc. Natl. Acad. Sci. 109, 9755–9760.
Berger, A.L., 1978. Long-term variations of caloric insolation resulting from the Earth's orbital elements. Quat. Res. 9, 139–167.
Brady, E.C., Otto-Bliesner, B.L., 2011. The role of meltwater-induced subsurface ocean warming in regulating the Atlantic meridional overturning in glacial climate simulations. Clim. Dyn. 37, 1517–1532.
Brennan, C.E., Meissner, K.J., Eby, M., Hillaire-Marcel, C., Weaver, A.J., 2013. Impact of sea ice variability on the oxygen isotope content of seawater under glacial and interglacial conditions. Paleoceanography 28, 388–400.
Brennan, C.E., Weaver, A.J., Eby, M., Meissner, K.J., 2012. Modelling oxygen isotopes in the university of Victoria earth system climate model for pre-industrial and last glacial maximum conditions. Atmos. Ocean 50, 447–465.
Broecker, W.S., Peteet, D.M., Rind, D., 1985. Does the ocean-atmosphere system have more than one stable mode of operation? Nature 315, 21–26.
Caniupán, M., Lamy, F., Lange, C.B., Kaiser, J., Arz, H., Kilian, R., Baeza Urrea, O., Aracena, C., Hebbeln, D., Kissel, C., et al., 2011. Millennial-scale sea surface temperature and Patagonian Ice Sheet changes off southernmost Chile (53°S) over the past ~ 60 kyr. Paleoceanography 26, PA3221.
Charles, C.D., Fairbanks, R.G., 1990. Glacial to interglacial changes in the isotopic gradients of Southern Ocean surface water. In: Geological History of the Polar Oceans: Arctic versus Antarctic. Springer, pp. 519–538.
Cortijo, E., Labeyrie, L., Vidal, L., Vautravers, M., Chapman, M., Duplessy, J.-C., Elliot, M., Arnold, M., Turon, J.-L., Auffret, G., 1997. Changes in sea surface hydrology associated with Heinrich event 4 in the North Atlantic Ocean between 40 and 60 N. Earth Planet. Sci. Lett. 146, 29–45.
Craig, H., 1957. Isotopic standards for carbon and oxygen and correction factors for mass-spectrometric analysis of carbon dioxide. Geochim. Cosmochim. Acta 12, 133–149.

Dickson, A.J., Austin, W.E.N., Hall, I.R., Maslin, M.A., Kucera, M., 2008. Centennial-scale evolution of Dansgaard-Oeschger events in the northeast Atlantic Ocean between 39.5 and 56.5 ka BP. Paleoceanography 23, PA3206.
Dokken, T.M., Jansen, E., 1999. Rapid changes in the mechanism of ocean convection during the last glacial period. Nature 401, 458–461.
van Donk, J., Mathieu, G., 1969. Oxygen isotope compositions of foraminifera and water samples from the Arctic Ocean. J. Geophys. Res. 74, 3396–3407.
Eby, M., Zickfeld, K., Montenegro, A., Archer, D., Meissner, K.J., Weaver, A.J., 2009. Lifetime of anthropogenic climate change: millennial time scales of potential CO_2 and surface temperature perturbations. J. Clim. 22, 2501–2511.
Elliot, M., Labeyrie, L., Dokken, T., Manthé, S., 2001. Coherent patterns of ice-rafted debris deposits in the Nordic regions during the last glacial (10–60 ka). Earth Planet. Sci. Lett. 194, 151–163.
Eynaud, F., De Abreu, L., Voelker, A., Schönfeld, J., Salgueiro, E., Turon, J.-L., Penaud, A., Toucanne, S., Naughton, F., Sánchez Goñi, M.F., et al., 2009. Position of the Polar Front along the western Iberian margin during key cold episodes of the last 45 ka. Geochem. Geophys. Geosys. 10.
Ferguson, G., Jasechko, S., 2015. The isotopic composition of the Laurentide ice sheet and fossil groundwater. Geophys. Res. Lett. 42, 4856–4861.
Flückiger, J., Knutti, R., White, J.W., 2006. Oceanic processes as potential trigger and amplifying mechanisms for Heinrich events. Paleoceanography 21, PA2014.
Ganopolski, A., Rahmstorf, S., 2001. Rapid changes of glacial climate simulated in a coupled climate model. Nature 409, 153–158.
Hibler III, W.D., 1979. A dynamic thermodynamic sea ice model. J. Phys. Oceanogr. 9, 815–846.
Hillaire-Marcel, C., de Vernal, A., 2008. Stable isotope clue to episodic sea ice formation in the glacial North Atlantic. Earth Planet. Sci. Lett. 268, 143–150.
Hodell, D., Crowhurst, S., Skinner, L., Tzedakis, P.C., Margari, V., Channell, J.E.T., Kamenov, G., Maclachlan, S., Rothwell, G., 2013. Response of Iberian Margin sediments to orbital and suborbital forcing over the past 420 ka. Paleoceanography 28, 185–199.
Hodell, D.A., Channell, J.E.T., Curtis, J.H., Romero, O.E., Röhl, U., 2008. Onset of "Hudson strait" Heinrich events in the eastern North Atlantic at the end of the middle pleistocene transition ~(640 ka)? Paleoceanography 23, PA4218.
Hodell, D.A., Evans, H.F., Channell, J.E.T., Curtis, J.H., 2010. Phase relationships of North Atlantic ice-rafted debris and surface-deep climate proxies during the last glacial period. Quat. Sci. Rev. 29, 3875–3886.
Hunke, E.C., Dukowicz, J.K., 1997. An elastic-viscous-plastic model for sea ice dynamics. J. Phys. Oceanogr. 27, 1849–1867.
Jouzel, J., Masson-Delmotte, V., Cattani, O., Dreyfus, G., Falourd, S., Hoffmann, G., Minster, B., Nouet, J., Barnola, J.-M., Chappellaz, J., et al., 2007. Orbital and millennial Antarctic climate variability over the past 800,000 years. Science 317, 793–796.
Kalnay, E., Kanamitsu, M., Kistler, R., Collins, W., Deaven, D., Gandin, L., Iredell, M., Saha, S., White, G., Woollen, J., et al., 1996. The NCEP/NCAR 40-year reanalysis Project. Bull. Am. Meteorol. Soc. 77, 437–471.
Keigwin, L.D., Boyle, E.A., 1999. Surface and deep ocean variability in the northern Sargasso Sea during marine isotope stage 3. Paleoceanography 14, 164–170.
Knutti, R., Flückiger, J., Stocker, T.F., Timmermann, A., 2004. Strong hemispheric coupling of glacial climate through freshwater discharge and ocean circulation. Nature 430, 851–856.
Kohfeld, K.E., Fairbanks, R.G., Smith, S.L., Walsh, I.D., 1996. Neogloboquadrina pachyderma (sinistral coiling) as paleoceanographic tracers in polar oceans: evidence from Northeast Water Polynya plankton tows, sediment traps, and surface sediments. Paleoceanography 11, 679–699.
van Kreveld, S., Sarnthein, M., Erlenkeuser, H., Grootes, P., Jung, S., Nadeau, M.J., Pflaumann, U., Voelker, A., 2000. Potential links between surging ice sheets, circulation changes, and the Dansgaard-Oeschger Cycles in the Irminger Sea, 60–18 kyr. Paleoceanography 15, 425–442.
Kucera, M., 2007. Planktonic foraminifera as tracers of past oceanic environments. In: Hillaire-Marcel, C., De Vernal, A. (Eds.), Paleoceanography of the Late Cenozoic, Volume 1: Methods in Late Cenozoic PaleoceanographyElsevier, pp. 799–812.
Lewis, S.C., LeGrande, A.N., Kelley, M., Schmidt, G.A., 2010. Water vapour source impacts on oxygen isotope variability in tropical precipitation during Heinrich events. Clim. Past 6, 325–343.
Li, C., Battisti, D.S., Bitz, C.M., 2010. Can North Atlantic sea ice anomalies account for Dansgaard-Oeschger climate signals? J. Clim. 23, 5457–5475.
Lisiecki, L.E., Raymo, M.E., 2005. A Pliocene-Pleistocene stack of 57 globally distributed benthic $\delta^{18}O$ records. Paleoceanography 20, PA1003.
MacAyeal, D.R., 1993. Binge/purge oscillations of the Laurentide ice sheet as a cause of the North Atlantic's Heinrich events. Paleoceanography 8, 775–784.
Marchitto, T.M., Curry, W.B., Lynch-Stieglitz, J., Bryan, S.P., Cobb, K.M., Lund, D.C., 2014. Improved oxygen isotope temperature calibrations for cosmopolitan benthic foraminifera. Geochim. Cosmochim. Acta 130, 1–11.
Marcott, S.A., Clark, P.U., Padman, L., Klinkhammer, G.P., Springer, S.R., Liu, Z., Otto-Bliesner, B.L., Carlson, A.E., Ungerer, A., Padman, J., et al., 2011. Ice-shelf collapse from subsurface warming as a trigger for Heinrich events. Proc. Natl. Acad. Sci. 108, 13415–13419.
Margari, V., Skinner, L.C., Tzedakis, P.C., Ganopolski, A., Vautravers, M., Shackleton, N.J., 2010. The nature of millennial-scale climate variability during the past two glacial periods. Nat. Geosci. 3, 127–131.
Martrat, B., Grimalt, J.O., Shackleton, N.J., de Abreu, L., Hutterli, M.A., Stocker, T.F., 2007. Four climate cycles of recurring deep and surface water destabilizations on the Iberian margin. Science 317, 502–507.
van Meerbeeck, C.J., Renssen, H., Roche, D.M., et al., 2009. How did marine isotope stage 3 and last glacial maximum climates differ?–perspectives from equilibrium simulations. Clim. Past 5, 33–51.
Meissner, K.J., Eby, M., Weaver, A.J., Saenko, O.A., 2008. CO_2 threshold for millennial-scale oscillations in the climate system: implications for global warming scenarios. Clim. Dyn. 30, 161–174.
Meissner, K.J., McNeil, B.I., Eby, M., Wiebe, E.C., 2012. The importance of the terrestrial weathering feedback for multimillennial coral reef habitat recovery. Glob. Biogeochem. Cycles 26, GB3017.
Meissner, K.J., Schmittner, A., Wiebe, E.C., Weaver, A.J., 2002. Simulations of Heinrich events in a coupled ocean-atmosphere-sea ice model. Geophys. Res. Lett. 29, 1671–1674.
Meissner, K.J., Weaver, A.J., Matthews, H.D., Cox, P.M., 2003. The role of land surface dynamics in glacial inception: a study with the UVic Earth System Model. Clim. Dyn. 21, 515–537.
Meland, M.Y., Dokken, T.M., Jansen, E., Hevrøy, K., 2008. Water mass properties and exchange between the Nordic seas and the northern North Atlantic during the period 23–6 ka: benthic oxygen isotopic evidence. Paleoceanography 23, PA1210.
Menviel, L., Spence, P., England, M.H., 2015. Contribution of enhanced Antarctic Bottom Water formation to Antarctic warm events and millennial-scale atmospheric CO_2 increase. Earth Planet. Sci. Lett. 413, 37–50.
Menviel, L., Timmermann, A., Friedrich, T., England, M.H., 2014. Hindcasting the continuum of Dansgaard–Oeschger variability: mechanisms, patterns and timing. Clim. Past 10, 63–77.
NGRIP Dating Group, 2008. Data Contribution Series #2008-034 NOAA/NCDC Paleoclimatology Program. IGBP PAGES/World Data Center for Paleoclimatology, Boulder CO, USA.
Pacanowski, R.C., 1995. MOM 2, Documentation, User's Guide and Reference Manual, p. 3. GFDL Ocean Group Tech. Rep.
Pahnke, K., Zahn, R., 2005. Southern Hemisphere water mass conversion linked with North Atlantic climate variability. Science 307, 1741–1746.
Peltier, W.R., Vettoretti, G., 2014. Dansgaard-Oeschger oscillations predicted in a comprehensive model of glacial climate: a kicked salt oscillator in the Atlantic. Geophys. Res. Lett. 41, 7306–7313.
Petersen, S.V., Schrag, D.P., Clark, P.U., 2013. A new mechanism for Dansgaard-Oeschger cycles. Paleoceanography 28, 1–7.
Rahmstorf, S., 1996. On the freshwater forcing and transport of the Atlantic thermohaline circulation. Clim. Dyn. 12, 799–811.
Rahmstorf, S., Feulner, G., Mann, M.E., Robinson, A., Rutherford, S., Schaffernicht, E.J., 2015. Exceptional twentieth-century slowdown in Atlantic Ocean overturning circulation. Nat. Clim. Change 5, 475480.
Rasmussen, T.L., Thomsen, E., 2004. The role of the North Atlantic Drift in the millennial timescale glacial climate fluctuations. Palaeogeogr. Palaeoclimatol. Palaeoecol. 210, 101–116.
Rasmussen, T.L., Thomsen, E., Labeyrie, L., van Weering, T.C.E., 1996. Circulation changes in the Faeroe-Shetland Channel correlating with cold events during the last glacial period (58–10 ka). Geology 24, 937–940.
Roche, D.M., Paillard, D., Caley, T., Waelbroeck, C., 2014. LGM hosing approach to Heinrich Event 1: results and perspectives from data–model integration using water isotopes. Quat. Sci. Rev. 106, 247–261.
Sarnthein, M., Stattegger, K., Dreger, D., Erlenkeuser, H., Grootes, P., Haupt, B.J., Jung, S., Kiefer, T., Kuhnt, W., Pflaumann, U., et al., 2001. Fundamental modes and abrupt changes in North Atlantic circulation and climate over the last 60 ky–Concepts, reconstruction and numerical modeling. In: The Northern North Atlantic: a Changing Environment. Springer, pp. 365–410.
Schmittner, A., Oschlies, A., Matthews, H.D., Galbraith, E.D., 2008. Future changes in climate, ocean circulation, ecosystems, and biogeochemical cycling simulated for a business-as-usual CO_2 emission scenario until year 4000 AD. Glob. Biogeochem. Cycles 22.
Semtner Jr., A.J., 1976. A model for the thermodynamic growth of sea ice in numerical investigations of climate. J. Phys. Oceanogr. 6, 379–389.
Shackleton, N.J., 1974. Attainment of isotopic equilibrium between ocean water and the benthonic foraminifera genus Uvigerina: isotopic changes in the ocean during the last glacial. Colloq. Int. Du. C.N.R.S. 219, 203–210.
Shackleton, N.J., Hall, M.A., Vincent, E., 2000. Phase relationships between millennial-scale events 64,000–24,000 years ago. Paleoceanography 15, 565–569.
Siddall, M., Rohling, E.J., Thompson, W.G., Waelbroeck, C., 2008. Marine isotope stage 3 sea level fluctuations: data synthesis and new outlook. Rev. Geophys. 46, RG4003.
Spence, P., Saenko, O.A., Sijp, W., England, M.H., 2013. North Atlantic climate response to Lake Agassiz drainage at coarse and ocean eddy-permitting resolutions. J. Clim. 26, 2651–2667.
Stouffer, R.J., Yin, J., Gregory, J.M., Dixon, K.W., Spelman, M.J., Hurlin, W., Weaver, A.J., Eby, M., Flato, G.M., Hasumi, H., et al., 2006. Investigating the causes of the response of the thermohaline circulation to past and future climate changes. J. Clim. 19, 1365–1387.
Voelker, A.H.L., de Abreu, L., 2011. A review of abrupt climate change events in the northeastern Atlantic Ocean (Iberian Margin): latitudinal, longitudinal, and vertical gradients. Abrupt Clim. Change Mech. Patterns Impacts 15–37.
Voelker, A.H.L., Lebreiro, S.M., Schönfeld, J., Cacho, I., Erlenkeuser, H., Abrantes, F., 2006. Mediterranean outflow strengthening during northern hemisphere coolings: a salt source for the glacial Atlantic? Earth Planet. Sci. Lett. 245, 39–55.

WAIS Divide Project Members, 2015. Precise interpolar phasing of abrupt climate change during the last ice age. Nature 520, 661–665.
Weaver, A.J., Eby, M., Wiebe, E.C., Bitz, C.M., Duffy, P.B., Ewen, T.L., Fanning, A.F., Holland, M.M., MacFadyen, A., Matthews, H.D., et al., 2001. The UVic Earth System Climate Model: model description, climatology, and applications to past, present and future climates. Atmos. Ocean 39, 361–428.
Wunsch, C., 2006. Abrupt climate change: an alternative view. Quat. Res. 65, 191–203.

Further reading

Barker, S., Diz, P., Vautravers, M.J., Pike, J., Knorr, G., Hall, I.R., Broecker, W.S., 2009. Interhemispheric Atlantic seesaw response during the last deglaciation. Nature 457, 1097–1102.
Blunier, T., Chappellaz, J., Schwander, J., Dällenbach, A., Stauffer, B., Stocker, T.F., Raynaud, D., Jouzel, J., Clausen, H.B., Hammer, C.U., et al., 1998. Asynchrony of Antarctic and Greenland climate change during the last glacial period. Nature 394, 739–743.
Clark, P.U., Hostetler, S.W., Pisias, N.G., Schmittner, A., Meissner, K.J., 2007. Mechanisms for an ~ 7-kyr climate and sea-level oscillation during marine isotope stage 3. Geophys. Monogr. Ser. 173, 209–246.
Hillaire-Marcel, C., De Vernal, A., Polyak, L., Darby, D., 2004. Size-dependent isotopic composition of planktic foraminifers from Chukchi Sea vs. NW Atlantic sedimentsimplications for the Holocene paleoceanography of the western Arctic. Quat. Sci. Rev. 23, 245–260.
Huiskamp, W.N., Meissner, K.J., 2012. Oceanic carbon and water masses during the Mystery Interval: a model-data comparison study. Paleoceanography 27, PA4206.
Kageyama, M., Merkel, U., Otto-Bliesner, B., Prange, M., Abe-Ouchi, A., Lohmann, G., Ohgaito, R., Roche, D.M., Singarayer, J., Swingedouw, D., et al., 2013. Climatic impacts of fresh water hosing under Last Glacial Maximum conditions: a multi-model study. Clim. Past 9, 935–953.
Lee, S.-Y., Chiang, J.C.H., Matsumoto, K., Tokos, K.S., 2011. Southern Ocean wind response to North Atlantic cooling and the rise in atmospheric CO_2: modeling perspective and paleoceanographic implications. Paleoceanography 26, PA1214.
Menviel, L., Timmermann, A., Timm, O.E., Mouchet, A., 2011. Deconstructing the Last Glacial termination: the role of millennial and orbital-scale forcings. Quat. Sci. Rev. 30, 1155–1172.
Okazaki, Y., Timmermann, A., Menviel, L., Harada, N., Abe-Ouchi, A., Chikamoto, M.O., Mouchet, A., Asahi, H., 2010. Deepwater formation in the North Pacific during the last glacial termination. Science 329, 200–204.
Saenko, O.A., Schmittner, A., Weaver, A.J., 2004. The Atlantic-pacific seesaw. J. Clim. 17, 2033–2038.
Stenni, B., Buiron, D., Frezzotti, M., Albani, S., Barbante, C., Bard, E., Barnola, J.M., Baroni, M., Baumgartner, M., Bonazza, M., et al., 2011. Expression of the bipolar see-saw in Antarctic climate records during the last deglaciation. Nat. Geosci. 4, 46–49.
Timmermann, A., Menviel, L., Okumura, Y., Schilla, A., Merkel, U., Timm, O., Hu, A., Otto-Bliesner, B., Schulz, M., 2010. Towards a quantitative understanding of millennial-scale Antarctic warming events. Quat. Sci. Rev. 29, 74–85.